El siguiente artículo fue publicado en Revista de la Academia Colombiana de Ciencias Exactas, Físicas y Naturales*, 39: 77-83 (2015);* y lo puede consultar en http://dx.doi.org/10.18257/raccefyn.252

Rev. Acad. Colomb. Cienc. Ex. Fis. Nat. 39(Supl.):77-83, 2015
doi: http://dx.doi.org/10.18257/raccefyn.252

Photoanodes modified with reduced graphene oxide to enhance photoelectrocatalytic performance of B-TiO_2 under visible light

Andrés Fabián Gualdrón-Reyes[1], Angel M. Meléndez[2,*], Martha Eugenia Niño-Gómez[1,2], Vicente Rodríguez-González[3], María Isabel Carreño-Lizcano[1]

[1]Centro de Investigaciones en Catálisis (CICAT)
[2]Centro de Materiales y Nanociencias (CMN), Universidad Industrial de Santander, Piedecuesta, Santander, Colombia
[3]División de Materiales Avanzados, Instituto Potosino de Investigación Científica y Tecnológica, San Luis Potosí, México

Abstract

The effect of reduced graphene oxide (rGO) content in boron-modified TiO_2 nanocrystalline films on their photocatalytic activity in phenol oxidation is investigated. Visible-light-active TiO_2 modified photoanodes were prepared by incorporating graphene sheets into the sol-gel reaction of B-TiO_2, followed by depositing the reaction products on 304 stainless steel plates by dip-coating technique. Thin films obtained by in situ sol-gel synthesis were characterized by FESEM, GIXRD and UV–vis diffuse reflectance spectroscopy. FESEM examination showed cracked films due to the tensile stress generated by solvent evaporation. GIXRD results showed that boron in the films inhibits the growth of crystallites. Comparing to unmodified TiO_2, B-TiO_2/rGO showed a red shift in the band gap. The potentiodynamic anodic polarization measurements showed that graphene incorporation improved the photogenerated electron transport within the film, hence increasing the photocurrent. These enhancements are explained on the basis of the ability of graphene in promoting the charge carrier separation by transferring the photogenerated electrons from the illuminated photoanode to the substrate. The film B-TiO_2/rGO obtained from the sol solution containing 0.03 wt/v% boron and 3 wt/v% graphene exhibited the highest photocurrent, which was 30 times larger compared with the photocurrent of TiO_2 film.

Key words: Composite thin films, modified TiO_2 photoelectrode, graphene, electron transport, photoelectrocatalytic oxidation.

Fotoánodos modificados con óxido de grafeno reducido para mejorar el rendimiento fotoelectrocatalítico de B-TiO_2 bajo luz visible

Resumen

Se investiga el efecto del contenido de óxido de grafeno reducido (rGO) en películas de TiO_2 modificadas con boro sobre su actividad fotocatalítica en la oxidación de fenol. Fotoánodos modificados de TiO_2 activos a la luz visible fueron preparados incorporando hojas de grafeno en la reacción sol-gel de B-TiO_2, seguido por el depósito de los productos de la reacción sobre láminas de acero inoxidable 304 por la técnica dip-coating. Las películas delgadas obtenidas por síntesis sol-gel *in-situ* fueron caracterizadas por FESEM, GIXRD y espectroscopia de reflectancia difusa UV-vis. La observación por FESEM mostró películas agrietadas debido al estrés mecánico generado por la evaporación del solvente. Los resultados de GIXRD mostraron que el boro en las películas inhibe el tamaño de los cristalitos. Comparando con el TiO_2, el dióxido de titanio modificado presentó un desplazamiento de la banda de energía prohibida hacia el rojo. Las mediciones de polarización anódica potenciodinámica mostraron que la incorporación de grafeno mejora el transporte de electrones fotogenerados dentro de las películas compuestas incrementando así la fotocorriente. Estas mejoras se explican en base a la habilidad del grafeno para facilitar la separación de portadores de carga, transfiriendo los electrones fotogenerados desde la película iluminada de B-TiO_2 hasta el sustrato. La película compuesta B-TiO_2/rGO obtenida a partir de la solución con 0.03 % p/v de boro y 3 % p/v de grafeno presentó la fotocorriente más alta, la cual fue 30 veces mayor comparada con la fotocorriente de la película de TiO_2.

Palabras clave: películas delgadas de materiales compuestos, fotoelectrodos modificados de TiO_2, grafeno, transporte electrónico, oxidación fotoelectrocatalítica.

Correspondencia:
Angel M. Meléndez, angelemet@gmail.com
Recibido: 30 de junio de 2015
Aceptado: 9 de septiembre de 2015

Introduction

In photoelectrocatalytic (PEC) and photovoltaic processes, titanium dioxide is widely used as photoanode material on conductive substrates (**Berger**, **Monllor-Satoca**, **Jankulovska, Lana-Villarreal**, Gómez, 2010). When TiO_2 is illuminated electron/hole (e^-/h^+) pairs are generated. Holes are accumulated in the semiconductor while the electrons are transported from TiO_2/solution interface to substrate. Subsequently, electrons are transported through the external circuit of the cell toward the cathode, thereby generating a photocurrent (**Gerischer**, 1990). A main inconvenient with TiO_2 is that only is active under UV light irradiation, limiting its PEC performance. Modification of TiO_2 can extend the light absorption to the visible region allowing the utilization of the sunlight (**Akpan**, **Hameed**, 2010). Titanium dioxide films have been conventionally prepared from nanoparticles suspension, but these materials exhibit low adherence due to particle detachment (**Krýsa, *et al.,*** 2006; **Castellano-Leal**, Córdoba, **Meléndez**, 2012; **Wang, Ao, Wang, Hou, Qian,** 2012). Instead, films preparation from the TiO_2 sol solutions can enhance the homogeneity and adherence of the film on the substrate. Nevertheless, if the electrode material is a nanoparticulated film, then the tortuous path that the electrons must follow through the nanoparticles hinders the electron transport, due to the presence of a high surface states density in the grain boundaries, thereby decreasing the photocurrent (**Villarreal, Mao, Wong, Gómez,** 2010; **Castellano-Leal, Córdoba, Meléndez,** 2012). Therefore, improvement of the electron transport within the TiO_2 is essential to increase the efficiency of electron collection.

Many alternatives have been proposed to enhance electron transport, such as the preparation of TiO_2 nanotubes to address the electron path (**Macak, *et al.,*** 2007) and the use of composite metal oxides (e.g. core shell) with matched band gaps (**Ramírez-Ortega, Meléndez, Acevedo-Peña, González, Arroyo,** 2014). Recently, incorporation of graphene sheets in TiO_2 nanoparticles has shown an improvement in the electron transport, increasing its PEC activity (**Bell, *et al.,*** 2011; **Wang, Li, Chen, Tao,** 2012). The excellent electronic conductivity of graphene endowed by its π-π conjugation structure, small particle size, and high specific surface area, becomes a convenient material to modified TiO_2 nanoparticles increasing the electron transport (**Bell, *et al.,*** 2011, **Wang, Ao, Wang, Hou, Qian,** 2012). Herein, B-TiO_2/rGO films deposited on 304 stainless steel plates were prepared by sol-gel method and deposited by dip-coating technique. rGO was incorporated in sol-gel TiO_2 thin films to enhance the electron transport. In addition, boron was added to the films to shift the TiO_2 photoresponse into the visible region. In order to prove whether the photocurrent response of TiO_2 can be enhanced under visible light illumination, phenol oxidation on B-TiO_2/graphene composite electrode was performed.

Materials and methods

All reagents were analytical reagent grade. All the solutions were prepared from Milli-Q deionized water (18.2 MΩ).

Synthesis of graphene

The general procedure for producing graphene oxide by the Hummers method has been described elsewhere (**Martínez-Orozco, Rosu, Lee**, **Rodríguez-González**, 2013). Briefly, graphene oxide GO was obtained by oxidation of graphite powder. The graphene oxide was dispersed in deionized water, 0.5 wt%. The exfoliation of GO was achieved using an ultrasound bath during 30 min. For reduction of GO (**Li, Muller**, **Gilje**, **Kanerand**, **Wallace**, 2008), a homogeneous dispersion of 0.05 wt% GO in deionized water (5.0 mL) was mixed with 5.0 mL of water, 5.0 mL of 35 wt% hydrazine and 35.0 mL of 28 wt% ammonia solution. After being vigorously stirred for a few minutes, the mixture was put in a water bath at 98°C during 1 h. The excess of hydrazine in the resulting dispersions was removed by exhaustive washing with deionized water using a vacuum system with a nylon membrane (0.45 μm pore size).

Preparation of modified TiO_2 films

TiO_2 sols with different boron and rGO content were obtained by dispersing rGO sheets in B-TiO_2 sols. Dispersions of (1, 2, 3 and 4) wt/v% rGO in ethanol were obtained using an ultrasound. A mixture of titanium butoxide and acetylacetone was added (molar ratio 1.0:0.5) into each rGO suspension under vigorous stirring at room temperature during 1 h, and a stable sol was achieved. Boric acid was added in different weight ratios (0.1, 0.2, 0.3) wt/v%. Thus, corresponding weight ratio of added boron was (0.017, 0.028, 0.038) wt/v%.

304 stainless steel plates (20 mm x 40 mm x 2 mm) were polished successively using emery papers of 120, 240, 320 and 600 grade. Plates were cleaned using an ultrasonic bath with ethanol and acetone. TiO_2 films with different boron and rGO content were deposited by dip-coating at a rate of 60 mm/min, followed by dehydration at 100°C for 10 min. This procedure was repeated 3 times to obtain three-layer films. Films were calcined by heating to 400°C at a rate of 3 deg/min and held at this temperature for 90 min. In this way, TiO_2 films were doped from different weight ratios 0.02, 0.03 and 0.04wt/v% of boron, and containing different amounts 1, 2, 3 and 4 wt/v% of rGO.

Characterization of B-TiO_2/graphene composite films

The morphology of the composite films was analyzed by field emission scanning electron microscopy FESEM using a JOEL Quanta 650 FEG equipped with an EDAX Apollo X energy dispersive X-ray spectroscopy. The crystallinity of the materials was investigated with grazing incidence X-ray diffraction GIXRD in a Bruker D8 Discover diffractometer with Da Vinci geometry operated at 40 kV and 30 mA,

using Cu Kα radiation selected with Ni filter, in grazing incidence mode with a step of 0.015° and a counting time of 1.0 s per step. Diffuse reflectance spectra were recorded with a Shimadzu PC 2401 UV-vis spectrophotometer. A 304 stainless steel plate was used as a reference.

Photoelectrochemical measurements

Photoelectrochemical measurements of B-TiO_2/rGO composite films were performed in a three-electrode cell with a potentiostat AUTOLAB PGSTAT 302N and Nova 10.1 software. A graphite rod was used as counter electrode and an Ag/AgCl/KCl (3 mol/L) electrode in a Luggin capillary was used as reference electrode. Linear sweep voltammetry was recorded at a scan rate of 10 mVs^{-1} and each measurement was done in duplicate. The measurements were performed illuminating the films in 1 mM phenol and 0.1 M $HClO_4$. All the solutions were bubbled with nitrogen during 20 min to remove the dissolved oxygen. The visible light source was a 150 W metal halide lamp (Philips, MHN-TD) with UV-block. Electrochemical impedance spectroscopy measurements were carried out at open circuit potential, using a signal amplitude of 10 mV in a frequency range of 30 kHz to 0.1 Hz. All the electrochemical experiments were performed at room temperature. After an evaluation of photoelectrochemical responses [**Gualdrón**, 2014], composite TiO_2 film prepared from 0.03 wt/v% B in the sol solution was the material with the best photoelectrochemical response, hence only are presented the results of this modification.

Results and discussion

Graphene characterization

Figure 1 show the characteristic XRD pattern of the as-prepared graphene oxide GO (which was produced by chemical oxidation of graphite) and the pattern after its reduction with hydrazine. The XRD profile of GO exhibits a strong peak at a Bragg angle of 2θ = 10.86°, corresponding to the 002 reflection of stacked GO sheets. The peak located at 2θ of ~26º in Figure 1a correspond to 002 reflection of graphite (JCPDS 75-1621). This result may be due to incomplete oxidation of graphite in synthesis procedure (**McAllister,** 2007). The broadening and asymmetry of 101 reflection (2θ = 42.5º) indicates the presence of turbostratic disorder in layers stacking (turbostrate carbon) (**Zaikovskii,** *et. al., 2012)*. After the reduction treatment, the 002 reflection of GO disappears (Figure 1b), and the characteristic peaks of rGO appear at 25.94º, 23.85° and 21.25°. The interlayer distance calculated from these peaks corresponding to 4.2 Å, 3.7 Å and 3.4 Å, respectively. These results indicates that the interlayer space between the graphene sheets was decreased by removing intercalated water molecules, and the oxygen-containing groups, during the hydrazine reduction process.

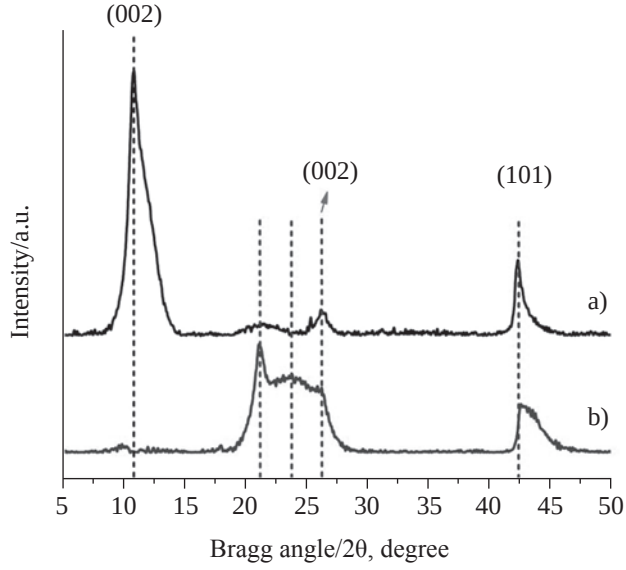

Figure 1. XRD profiles of (a) graphene oxide GO and (b) reduced graphene oxide rGO obtained after 1 h of hydrazine-reduction treatment of GO.

It is well known that titanium dioxide exhibit low conducting properties, which can restrain the photogenerated electron transport from the film to the substrate, hence decreasing the generated photocurrent. In order to increase the conductivity in the films, and promote the electron transport from the interface modified-TiO_2/electrolyte to the substrate, rGO was incorporated in the films.

Morphological, structural and optical properties

Figure 2 shows FESEM images of titanium dioxide films. The average thickness for TiO_2, B-TiO_2 and B-TiO_2/rGO (3 wt/v% rGO loading) films was approximately 288 nm, 159 nm and 168 nm, respectively. Boron doping promotes a high number of cracks than TiO_2 film. The cracked morphology can be associated to tensile stress generated by capillary pressure resulting from the solvent evaporation. Solvent evaporation rate is low as the thickness increases and hence the number of cracks diminishes (**Jing**, **Zhao**, **Zhang**, 2007). EDS mapping of B-TiO_2/rGO film (Figure 3) shows a homogeneous distribution of Ti, O, B, and C in the film. The limited number of points for Ti analysis in the cracks (dark zones) is due to a low amount of TiO_2 covering the stainless steel support, which is composed of Fe, Cr and Ni.

Figure 4 shows the GIXRD patterns of the different films. Only the characteristics reflections (101), (004), (200), (105) and (211) of anatase phase (JCPDS 211272) were observed. Diffraction peaks of modified films are wider and less intense than unmodified TiO_2 film. Assuming a spherical shape for the particles, the crystallite size (D) was calculated using the Scherrer equation (eq. 1)

$$D = \frac{0.89\lambda}{\beta\cos\theta} \quad (1)$$

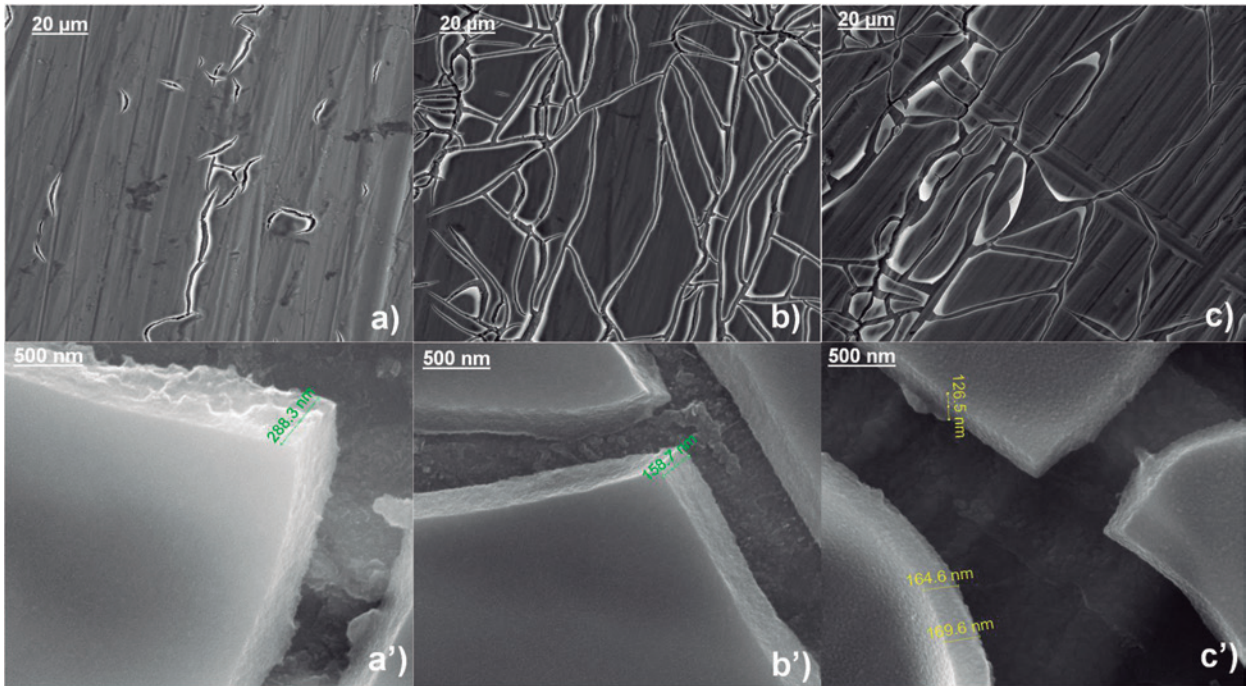

Figure 2. Typical FESEM images (5000x) of a) TiO_2, b) B-TiO_2 and c) B-TiO_2/rGO films, and their corresponding magnifications a'-c') at 150000x.

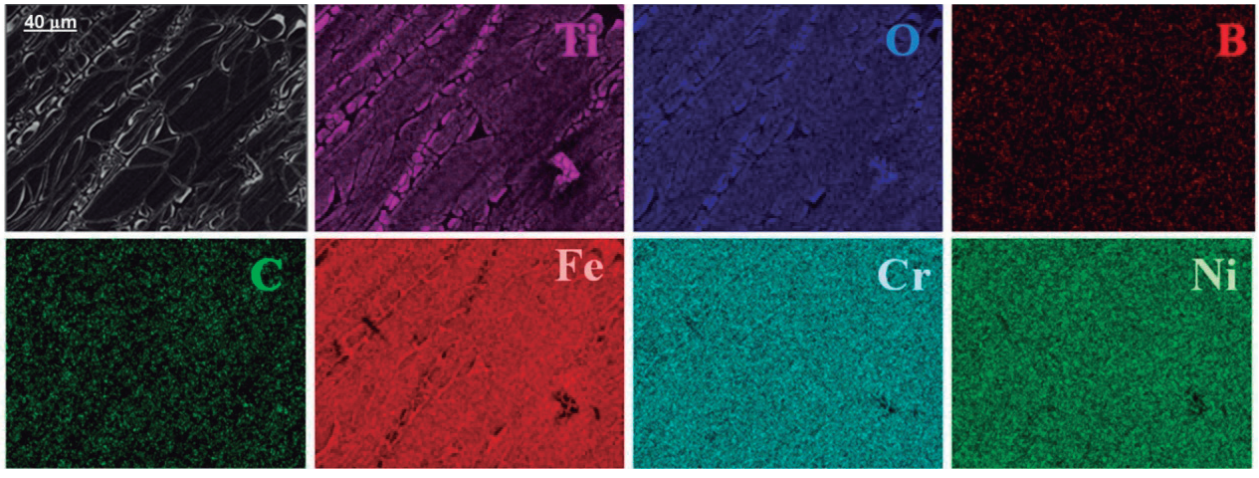

Figure 3. Representative FESEM-EDS mapping analysis of a photocatalytic film of B-TiO_2/rGO supported on a stainless steel substrate.

where, λ is the X-ray wavelength of Cu Kα radiation 0.15406 nm, β is the full width at half maximum (FWHM) of (101) anatase peak, and θ is the Bragg angle (**Ramírez-Ortega, Meléndez, Acevedo-Peña, González, Arroyo,** 2014). Average crystallite sizes for TiO_2, B-TiO_2 and B-TiO_2/rGO films are 18.94 nm, 11.60 nm and 13.94 nm, indicating that boron doping inhibits the growth of TiO_2 crystallites. Diffraction peaks of the different films (Figure 4) not show displacements of the Bragg angles. It is due to the ionic radius of B^{3+} (0.23 Å) is much smaller than Ti^{4+} (0.64 Å), and then boron could be incorporated in interstitial positions within the TiO_2 lattice (**Lu, Tian, Chen, Zhang,** 2010).

Figure 5 displays the modified Kubelka-Munk function used for determination of band gaps of the different titanium dioxide films. The calculated band gap values for TiO_2, B-TiO_2 and B-TiO_2/rGO films were 3.28 eV, 2.72 eV and 2.63 eV respectively. Thereby, boron decreases the energy of ban gap towards the visible region. Incorporation of rGO also diminishes the ban gap, extending even more the light absorption to the visible region, suggesting a chemical interaction of B-TiO_2 with graphene sheets. It has been associated to the formation of impurity levels located below of the bottom of the conduction band of TiO_2 (**Ding, *et al.,*** 2009).

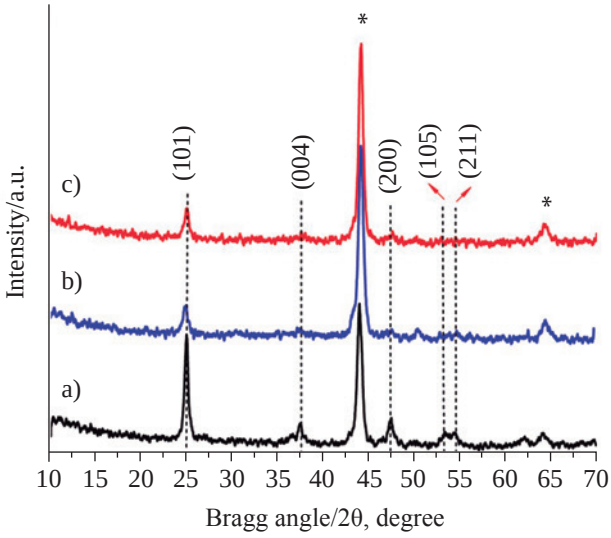

Figure 4. Typical GIXRD profiles of a) TiO_2, b) B-TiO_2 and c) B-TiO_2/rGO films. The asterisk corresponds to reflection of stainless steel substrate.

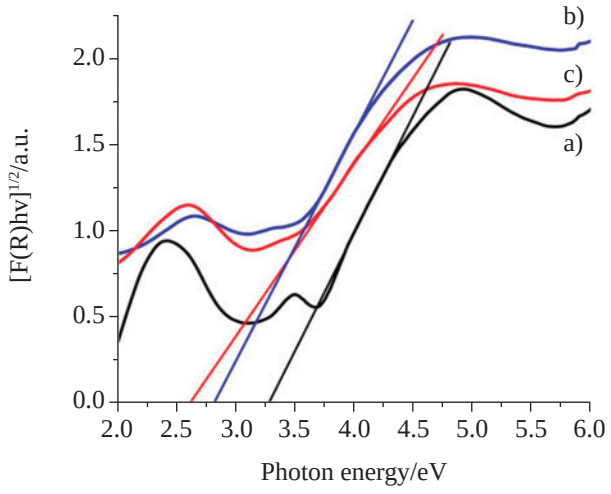

Figure 5. Schematic presentation of the method for band gap determination of a) TiO_2, b) B-TiO_2 and c) B-TiO_2/rGO (3 wt/v% rGO) films.

Photoelectrochemical properties

Figure 6(i) shows the potentiodynamic anodic polarization of TiO_2, B-TiO_2, and B-TiO_2/rGO films with different rGO load, illuminated under visible radiation, in 1 mM phenol using 0.1 M $HClO_4$ as supporting electrolyte. Unmodified TiO_2 showed negligible photocurrent in the potential window studied (Figure 6(i)-a). An increase in the content of graphene enhances the photoresponse until rGO content is 3 wt/v%. Thus, B-TiO_2/rGO film with 3 wt/v% rGO loading exhibited a photocurrent 30 higher than TiO_2 film. This indicates that more photogenerated electrons are transported from the film to the external circuit of the cell,

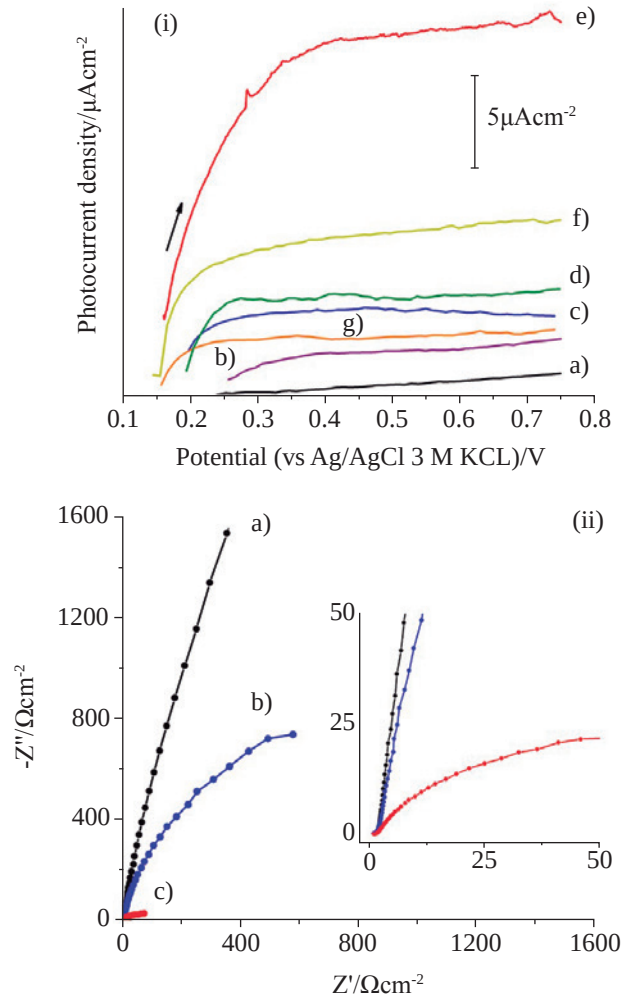

Figure 6. (i) Anodic polarization (10 mVs^{-1}) obtained in 1 mM phenol + 0.1 M $HClO_4$ under visible light for a) TiO_2 and b) B-TiO_2 films and B-TiO_2/r-GO composite films with different graphene content (wt %): c) 1, d) 2 , e) 3 , f) 4 and g) 10. (ii) Nyquist plots obtained under illumination for a) TiO_2, b) B-TiO_2 and c) B-TiO_2/rGO (3 wt/v% rGO loading) films in 0.1 M $HClO_4$ under visible light.

increasing the generated photocurrent (**Berger, Monllor-Satoca, Jankulovska, Lana-Villarreal, Gómez,** 2010; **Castellano-Leal, Córdoba, Meléndez,** 2012).

An increasing in the rGO content after 3 wt/v% did not improve the photoresponse, on the contrary photocurrent decreases. When the graphene content exceeded 3 wt/v%, redundant rGO can acts as a recombination center restraining the electron transport, or decreasing the passage of light through the film. Whereas the electrons are transported towards the external circuit of the cell, the photogenerated holes can react with adsorbed H_2O molecules in the film forming hydroxyl radicals as follows (eq. 2-4) (**Comninellis,** 1994):

$$B–TiO_2 + h^+ + H_2O \rightarrow B–TiO_2\,[HO^{\cdot}] + H^+ \qquad (2)$$

thereby, phenol (R) is oxidized (RO) on the film surface

$$B–TiO_2\,[HO^{\bullet}] + R \rightarrow B–TiO_2 + RO + H^+ + e^- \quad (3)$$

Or can be oxidized directly by the holes with formation of radical cations:

$$B–TiO_2 + h^+ + R \rightarrow B–TiO_2 + R^{\cdot +} \rightarrow \text{degradation products} \quad (4)$$

Therefore, phenol oxidation can be photodegradate by indirect (production of hydroxyl radicals, eqs. 2 and 3) or direct reactions (hole transfer, eq. 4).

To explain the increase in electron transport inside the films with the incorporation of rGO, electrochemical impedance spectroscopy (EIS) was performed under visible illumination at open-circuit potential. Figure 6(ii) exhibits the typical Nyquist plots of TiO_2, B-TiO_2 and B-TiO_2/rGO films. The curvature radius of the Nyquist plot decreases in the following order TiO_2 > B-TiO_2 > B-TiO_2/rGO indicating that the resistance of the films is diminished with introducing rGO. Therefore, the improved voltammetry–photocurrent responses of the composite films showed in Figure 6(i)a is explained by fast interfacial charge transfer, which induce effective separation of photoinduced charge carriers.

It has been found that when stainless steel is coated with TiO_2 via sol-gel dip coating method, TiO_2 film is unintentionally contaminated with metallic impurities from substrate, which caused a decrease in the photocatalytic activity of TiO_2 (**Fernández, *et al.,*** 1995; **Sokolov, *et al.,*** 2009). Photoelectrochemical oxidation experiments of cyanide (**Ardila-Alvarado, Fuentes-Torres,** 2012), copper(I)-cyanide (**Quesada-Plata, Quintero-Ruiz,** 2014) and phenol (**Joya-Herrera, Sequeda-Pico,** 2014), mostly carried out by our research group, have shown that if modified TiO_2 films are prepared on stainless steel by sol-gel dip coating, then the photocurrent response in photovoltammetry only appears at large anodic overpotentials, where the electrochemical oxidation of pollutant takes place. The aforementioned results confirm the poor photocatalytic activity of this type of photoelectrodes. Conversely, herein it is possible to observe a well-behaved photoelectrochemical process for a TiO_2 thin-film deposited on stainless steel by sol-gel dip coating (Figure 6i), which shows the benefits of incorporating rGO sheets into a B-TiO_2 nanoparticulate film. However, it has been found that the value of the photocurrent is lower than that observed for B-TiO_2 supported in a titanium plate (**Gualdrón-Reyes,** *et. al.*, 2014. Manuscript in preparation). Hence, the rate of photoelectrocatalytic oxidation of phenol on stainless steel coated with modified TiO_2 is lower than that of titanium. Current efforts are focused on avoid the contamination of TiO_2 film from metallic cations of stainless steel to improve the photocurrent generation.

Conclusions

B-TiO_2/rGO composite films deposited on stainless steel were successfully prepared by sol-gel method and dip-coating technique. Boron and rGO in the titanium dioxide films extended the light absorption to the visible region. The high photocurrent on the B-TiO_2/rGO photoelectrode was attributed to the improved electron transport inside the films, due to graphene acts as an efficient acceptor and transporter of photogenerated electrons, facilitating the electron transport from the film/electrolyte interface to the substrate and towards the external circuit of the cell. An excess of graphene content in composite films promotes the formation of recombination centers, decreasing the electron transport in the B-TiO_2/rGO films. The TiO_2-modified composite photoelectrode here developed enables that photogenerated electrons under visible-light irradiation can generate a photocurrent, although their magnitude is not so high in comparison with the same photoelectrode material supported on titanium due to the synthesis method.

Acknowledgments

This study has been financially supported by Universidad Industrial de Santander (project 5704). Andrés Gualdrón is grateful to COLCIENCIAS for the Msc. grant through the program Jóvenes investigadores 2013.

Conflict of interests

The authors declare no conflicts of interest of any kind.

References

Akpan, U.G., Hameed, B.H. 2010. The advancements in sol–gel method of doped-TiO_2 photocatalysts. *Appl. Catal. A-Gen.* **375:** 1-11.

Ardila-Alvarado, L.F., Fuente-Torres, S.N. 2012 (in Spanish). Electrochemical study of the degradation of cyanide on titanium dioxide films doped with nitrogen, N-TiO_2, under visible light. Undergraduate thesis. Industrial University of Santander, Colombia. p. 37, 38.

Bell, N.J., Ng, Y.H. Du, H., Coster, H., Smith, S.C., Amal, A. 2011. Understanding the enhancement in photoelectrochemical properties of photocatalytically prepared TiO_2-reduced graphene oxide composite. *J. Phys. Chem. C,* 2011, **115** (13): 6004-6009.

Berger, T., Monllor-Satoca, D., Jankulovska, Lana-Villarreal, M.T., Gómez, R. 2010. The electrochemistry of nano-structured titanium dioxide electrodes. *ChemPhysChem* **13:** 2824-2875.

Castellano-Leal, E.L., Córdoba, E., Meléndez, A.M. 2012 (in Spanish). *Effect of $TiO_{2x}N_x$ film thickness in electrophotocatalytic and photocatalytic degradation of methyl orange under visible-light illumination.* XXVII Congress of the Mexican Society of Electrochemistry -and- 5th Meeting of the ECS Mexican Section. Toluca, Mexico. p. 1-12.

Comninellis, C. 1994. Electrocatalysis in the electrochemical conversion/combustion of organic pollutants for waste water treatment. *Electrochim. Acta* **39** (11-12): 1857-1862.

Ding, J., Yuan, Y., Xu, J., Deng, J., Guo, J. 2009. TiO_2 nanopowder co-doped with iodine and boron to enhance visible-light photocatalytic activity. *J. Biomed. Nanotechnol.* **5:** 1-7.

Fernández, A., Lassaletta, G., Jiménez, V. M., Justo, A., González-Elipe, A. R., Herrmann, J.-M., Tahiri, H. Ait-Ichou, Y. 1995. Preparation and characterization of TiO_2 photocatalysts supported on various rigid supports (glass, quartz and stainless steel). Comparative studies of photocatalytic activity in water purification. *Appl. Catal. B: Environ.* **7:** 49-63.

Gerischer, H. 1990. The impact of semiconductors on the concepts of electrochemistry. *Electrochim. Acta* **35** (11-12): 1677-1699.

Gualdrón-Reyes, F.A. 2014. Photoelectrochemical phenol oxidation in aqueous solution by using boron-doped TiO_2/graphene films deposited on stainless steel. Master thesis. Industrial University of Santander, Colombia. p. 37-38.

Gualdrón-Reyes, F. A., Meléndez, A.M., González, I., Lartundo-Rojas, L., Niño-Gómez, M. 2014. The effect of substrate on the photo(electro)chemical properties and photocatalytic activity of TiO_2 photoanodes modified with boron and graphene. Manuscript in preparation.

Jing, C., Zhao, X., Zhang, Y. 2007. Sol–gel fabrication of compact, crack-free alumina film. *Mater. Res. Bull.* **42:** 600-608.

Joya-Herrera, L.M., Sequeda-Pico, J.A. 2014 (in Spanish). Evaluation of N-TiO_2 semiconductors films in the photoelectrocatalytic oxidation of phenol with visible light. Undergraduate thesis. Industrial University of Santander, Colombia. p. 40-44.

Krýsa, J., Waldner, G., Měšťánková, H., Jirkovský, J., Grabner, G. 2006. Photocatalytic degradation of model organic pollutants on an immobilized particulate TiO_2 layer. *Appl. Catal. B-Environ.* **64:** 290-301.

Li, D., Muller, M.B., Gilje, S., Kanerand, R.B., Wallace, G.G. 2008. Processable aqueous dispersions of graphene nanosheets. *Nat. Biotechnol.* **3:** 101-105.

Lu, X., Tian, B., Chen, F., Zhang, J. 2010. Preparation of boron-doped TiO_2 films by autoclaved-sol method at low temperature and study on their photocatalytic activity. *Thin Solid Films* **519:** 111-116.

Macak, J.M., Tsuchiya, H., Ghicov A., Yasuda, K., Hahn, R., Bauer, S., Schmuki, P. 2007. TiO_2 nanotubes: self-organized electrochemical formation, properties and applications. *Curr. Opin. Solid St. M. Sci.* **11:** 3-18.

McAllister, M.J., Li, J.L., Adamson, D.H., Schniepp, H.C., Abdala, A.A., Liu, J., Herrera-Alonso, M., Milius, D.L., Car, R., Prud'homme, R.K., Aksay, I.A. 2007. Single sheet functionalized graphene by oxidation and thermal expansion of graphite. *Chem. Mater.* **19:** 4396-4404.

Martínez-Orozco, R.D., Rosu, H.C., Lee, S.W., Rodríguez-González, V. 2013. Understanding the adsorptive and photoactivity properties of Ag-graphene oxide nanocomposites. *J. Hazard. Mater.* **263:** 52-60.

Quesada-Plata, F.E., Quintero-Ruiz, J.A. 2014 (in Spanish). Electrochemical study of the effect of copper(I) as catalyst for oxidation of cyanide under visible light using titanium oxide films doped with nitrogen. Undergraduate thesis. Industrial University of Santander, Colombia. p. 37-43.

Ramírez-Ortega, D., Meléndez, A. M., Acevedo-Peña, P., González, I., Arroyo, R. 2014. Semiconducting properties of ZnO/TiO_2 composites by electrochemical measurements and their relationship with photocatalytic activity. *Electrochim. Acta,* **140:** 541-549.

Lana-Villarreal, M.T., Mao, Y., Wong, S.S., Gómez, R. 2010. Photoelectrochemical behavior of anatase nanoporous films: effect of the nanoparticle organization. *Nanoscale,* **2:** 1690-1698.

Sokolov, S., Ortel, E., Radnik, J., Kraehnert, R. 2009. Influence of steel composition and pre-treatment conditions on morphology and microstructure of TiO_2 mesoporous layers produced by dip coating on steel substrates *Thin Solid Films,* **518:** 27-35.

Wang, P., Ao, Y., Wang, C., Hou, J., Qian, J. 2012. Enhanced photoelectrocatalytic activity for dye degradation by graphene–titania composite film electrodes. *J. Hazard. Mater.* **223-224:** 79-83.

Wang, D., Li, X., Chen, J., Tao, X. 2012. Enhanced photoelectrocatalytic activity of reduced graphene oxide/TiO_2 composite films for dye degradation. *Chem. Eng. J.* **198-199:** 547-554.

Zaikovskii, A.V., Mal'tsev, V.A., Novopashin, S.A., Sakhapov, S.Z., Smovzh, D.V. 2012. Synthesis of nanocrystalline carbon upon methane pyrolysis in arc discharge. *Nanotechnologies in Russia,* **7:** 11.